ACS APPLIED MATERIALS & INTERFACES
Research Article
www.acsami.org

Controlling Work Function and Damaging Effects of Sputtered RuO_2 Gate Electrodes by Changing Oxygen Gas Ratio during Sputtering

Hyo Kyeom Kim,[†] Il-Hyuk Yu,[‡] Jae Ho Lee,[‡] Tae Joo Park,[§] and Cheol Seong Hwang*[,†,‡]

[†]Department of Nano Science and Technology, Graduate School of Convergence Science and Technology, and [‡]WCU Hybrid Material Program, Department of Materials Science and Engineering and Inter-university Semiconductor Research Center, Seoul National University, Seoul 151-744, Korea

[§]Department of Materials Engineering, Hanyang University, Ansan 426-791, Korea

ABSTRACT: RuO_2 metal gates were fabricated by a reactive sputtering method under different O_2 gas ratios. For the given sputtering power of 60 W, a ~13% O_2 ratio was the critical level below or over which RuO_2 film has hyperstoichiometric and stoichiometric compositions, which resulted in a difference in the effective work function by ~0.2 eV. The stoichiometric RuO_2 film imposes almost no damaging effect to the underlying SiO_2 and HfO_2 gate dielectrics. The RuO_2 gate decreased the equivalent oxide thickness by ~0.5 nm and leakage current by around two orders of magnitude compared to the Pt-gated samples.

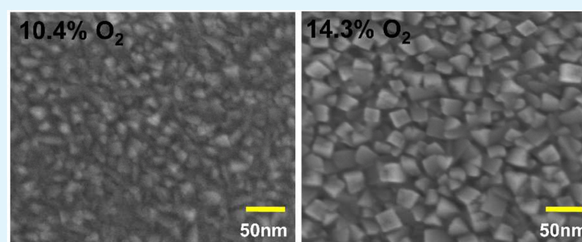

KEYWORDS: *ruthenium oxide, sputtering, metal gate, effective work function, oxygen ratio, high-k gate dielectric*

1. INTRODUCTION

The aggressive scaling of gate length in complementary metal oxide semiconductor field-effect transistors (CMOSFETs) recently has necessitated the equivalent oxide thickness (EOT) to decrease to far below 1 nm.[1] Given the slow adoption of higher-*k* dielectrics, such as La_2O_3, the importance of engineering gate electrodes for HfO_2, of which the dielectric constant (*k*) is only 17, is ever increasing. Besides the control of the effective work function (EWF) of the gate metal, an additional benefit for the EOT scaling has been acquired, in the form of a scavenging effect of the interfacial layer thanks to the higher chemical activity of several gate metals compared to Si.[2,3] However, the so-called dead-layer effect of the metal/high-*k* interface sets a fundamental barrier for the EOT scaling far below 1 nm.[4] Such a dead-layer effect is an intrinsic problem due to the finite screening length and the almost fully suppressed ionic polarization of metals, so that an alternative approach is necessary. The dead-layer effect originates fundamentally from the lack of neighboring dipoles outside the high-*k* dielectric film which would have enhanced the ionic polarization of the dielectric film even on the surface.

Conductive metal oxides, such as RuO_2, are intriguing materials in this regard; they have shown reasonably low resistivity (< ~100 $\mu\Omega$ cm), but their non-zero ionic bonding characteristic allows a (partial) polarization of the electrode, which largely suppresses the dead-layer effect.[5−7] Such a positive effect has been well demonstrated in metal-insulator (high-*k*)-metal (MIM) systems,[8] as well as metal-insulator (high-*k*)-semiconductor (MIS) systems,[9] where the adoption of an RuO_2 electrode results in the EOT decreasing by ~0.5 nm in the EOT range ≲2 nm. In addition, EWF of RuO_2 is quite large (>5.0 eV), making it suitable in p-type MOSFETs, which can also decrease the electron injection from the gate metal to dielectrics.

However, RuO_2 is a relatively unstable oxide because of its relatively small oxide formation energy compared with other dielectric oxides, so controlling the Ru:O ratio to the stoichiometry value is not a trivial task in the integrated structure. In addition, the hyperstoichiometric oxides (RuO_3 or RuO_4) could be formed relatively easily, making the process and material properties less reliable. This could especially be the case when the RuO_2 is fabricated by reactive sputtering, where the status of the metal target surface can be altered easily by the oxygen partial pressure (P_{O2}) in the sputtering. In general, there are two P_{O2} ranges in which the oxide films are formed according to the so-called generic curve.[10] When P_{O2} is higher or lower than a certain critical value, which depends on the sputtering power and total pressure, the oxide film grows via the sputtering of oxidized target, or sputtering of non-oxidized target, so that the oxide film is formed by the oxidation of metallic films on the substrate. These two process regimes could have a crucial influence on the structure and electrical properties of the growing RuO_2 film, which in turn influence the device performance of the MOSFET. In the previous work, only one oxygen gas ratio of 10.4% was adopted for preparing the RuO_2 film by the reactive sputtering, which may not correspond to the optimum growth condition for the optimum device performance.[9] As described above, the growth condition,

Received: November 6, 2012
Accepted: February 5, 2013
Published: February 5, 2013

© 2013 American Chemical Society

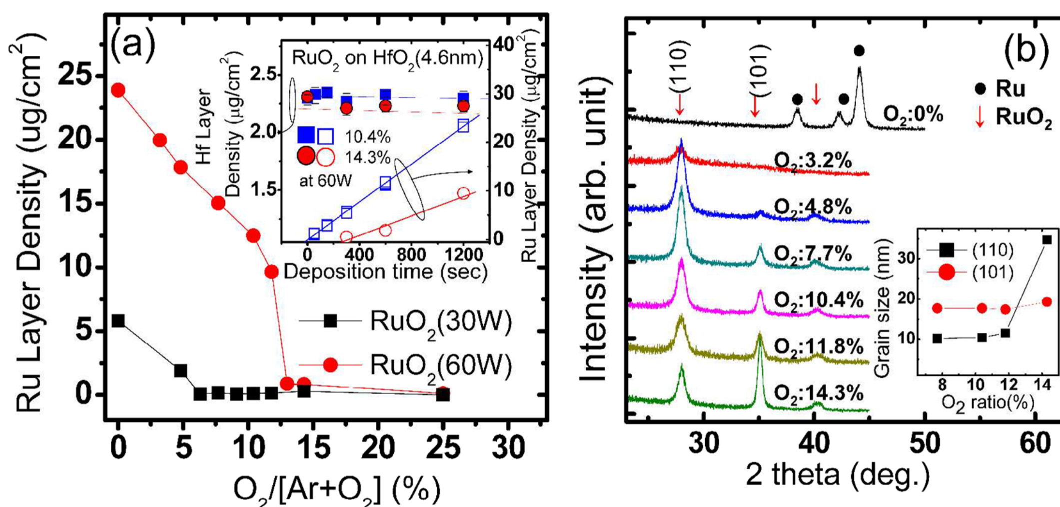

Figure 1. (a) Variations of Ru layer density of RuO_2 films at 30 and 60 W as a function of O_2 ratio and (inset) Hf layer density for a given HfO_2 thickness and Ru layer density as a function of deposition time of RuO_2 electrodes, and (b) GAXRD spectra of as-deposited Ru (~10 nm) and RuO_2 (~30 nm) with various O_2 ratios, and (inset) the variations in the grain size of the films estimated from the two XRD peaks using the Scherrer equation.

especially oxygen gas ratio, profoundly influence the growth behavior as well as the property of the RuO_2 film as the metal gate. In this work, therefore, RuO_2 gate electrodes were grown on terraced SiO_2 and HfO_2 film substrates under different P_{O2} conditions. The influences of growth conditions on the physical and electrical properties of the RuO_2 films as well as the performance of the MIS capacitors were carefully examined.

2. EXPERIMENTAL SECTION

Ru and RuO_2 films were grown by RF magnetron sputtering using a 3-inch-diameter Ru target (~99.9%) on thermal SiO_2 and HfO_2 dielectrics on p-type Si substrate using a shadow mask. In the RuO_2 sputtering process, the $O_2/(Ar+O_2)$ gas flow ratio (O_2 ratio) was varied from 3.3% to 16.7% by varying the O_2 gas flow rate from 1 sccm to 10 sccm for the given Ar gas flow rate of 30 sccm. For comparison, TiN films were grown at a DC power of 100 W using a 3-inch-diameter Ti metal target (~99.99%) and 5% $N_2/(Ar+N_2)$ reactive gas. A Pt electrode was also fabricated by DC sputtering at DC power ranging from 10W to 100W. On all of the samples, in situ sputtered Pt layer (~50 nm) was grown for electrical measurements. The gate metal films were deposited at a substrate temperature of 40 °C. HfO_2 films were grown by an atomic layer deposition (ALD) method to a thickness in the range of 2−6 nm on an HF-cleaned p-type Si substrate (100) at 270 °C using tetrakis(ethylmethylamino)hafnium (Hf(N-$(CH_3)(C_2H_5))_4$) and ozone gas with a concentration of 170 g/Nm^3 as the Hf precursor and oxygen source, respectively. Terraced SiO_2 wafers were prepared by wet-etching of 8-nm-thick thermal SiO_2 using a dilute HF solution. Terraced SiO_2 wafer means the Si wafer coated with a SiO_2 layer, the thickness of which varies across the wafer.

The deposition rates of Ru and RuO_2 films were examined by X-ray fluorescence (XRF; Themoscientific, ARL Quant'x), and the crystallinity of the films was estimated by glancing angle X-ray diffraction (GAXRD, PANalytical X'Pert PRO MPD). The depth profiles of the atomic concentrations, chemical binding states, and microstructures of the films were analyzed by Auger electron spectroscopy (AES; Perkin-Elmer PHI 660), X-ray photoelectron spectroscopy (XPS; AXIS-His), and high-resolution transmission electron microscope (HRTEM; Tecnai F20, field-emission, 200 kV), respectively. To not induce any modification in the chemical states of the RuO_2, sputter cleaning method, using accelerated Ar^+ ion for XPS was not adopted. Although there could be some interference by the surface contamination, XPS still provides important information on the chemical status of the RuO_2 materials depending on the oxygen gas ratio.

After the gate electrode formation, forming gas (5% H_2/95% N_2) annealing was performed at 400 °C for 30 min. Capacitance−voltage ($C-V$) characteristics were examined using a Hewlett-Packard 4194A Impedance/Gain-Phase Analyzer at 100 kHz. The measured $C-V$ curves were simulated using Hauser's CVC program to obtain the flat band voltage (V_{FB}) and EOT values.[11]

3. RESULTS AND DISCUSSION

Figure 1a shows the variations of Ru layer density of RuO_2 films, estimated by XRF, for the two RF powers (30 and 60 W) as a function of O_2 ratio when the deposition was performed for 600 s. In both cases, the Ru layer density decreases almost linearly with the increasing O_2 ratio up to a certain critical value (~6 and 13% for 30 and 60 W, respectively), and then drops to a very low value. Such a behavior can be understood from the well-known behavior of reactive sputtering using a metal target, where the increasing reactive gas ratio (O_2 ratio in this case) poisons (oxidizes) the target surface.[12] Up to the critical O_2 ratio, the target surface maintains a metallic state so that the sputtered atoms are mostly metal, which then oxidize to the oxide film on the substrate. Increasing the O_2 ratio enhances the resputtering effect due to the bombardment of negatively charged oxygen ions on the growing film. In contrast, the Ru target surface is almost fully oxidized when the O_2 ratio is higher than the critical value, and sputtered materials are mostly oxidized Ru molecules, meaning that the oxidation of growing film on the substrate plays a relatively minor role. Because of the generally very low growth rate for the case of 30 W, the following experiments were performed with 60 W. The inset of Figure 1a shows the variations of the Ru layer density with the deposition time for the O_2 ratios of 10.4 and 14.3%, which are below and over the critical value, respectively. Although the data in Figure 1a showed a substantially different Ru layer density (a 15-fold difference) under these two O_2 ratios, the actual growth rate, calculated from the slopes in the inset figure, was not so different (by only a factor of 2), meaning that the high O_2 ratio condition induced a quite long induction time for the nucleation of the film. The inset figure also shows that the Hf layer density of the HfO_2 film beneath the RuO_2 with an O_2 ratio of 14.3% decreased slightly compared with that of 10.4% case, suggesting the HfO_2 films were slightly etched by 0.1−0.2

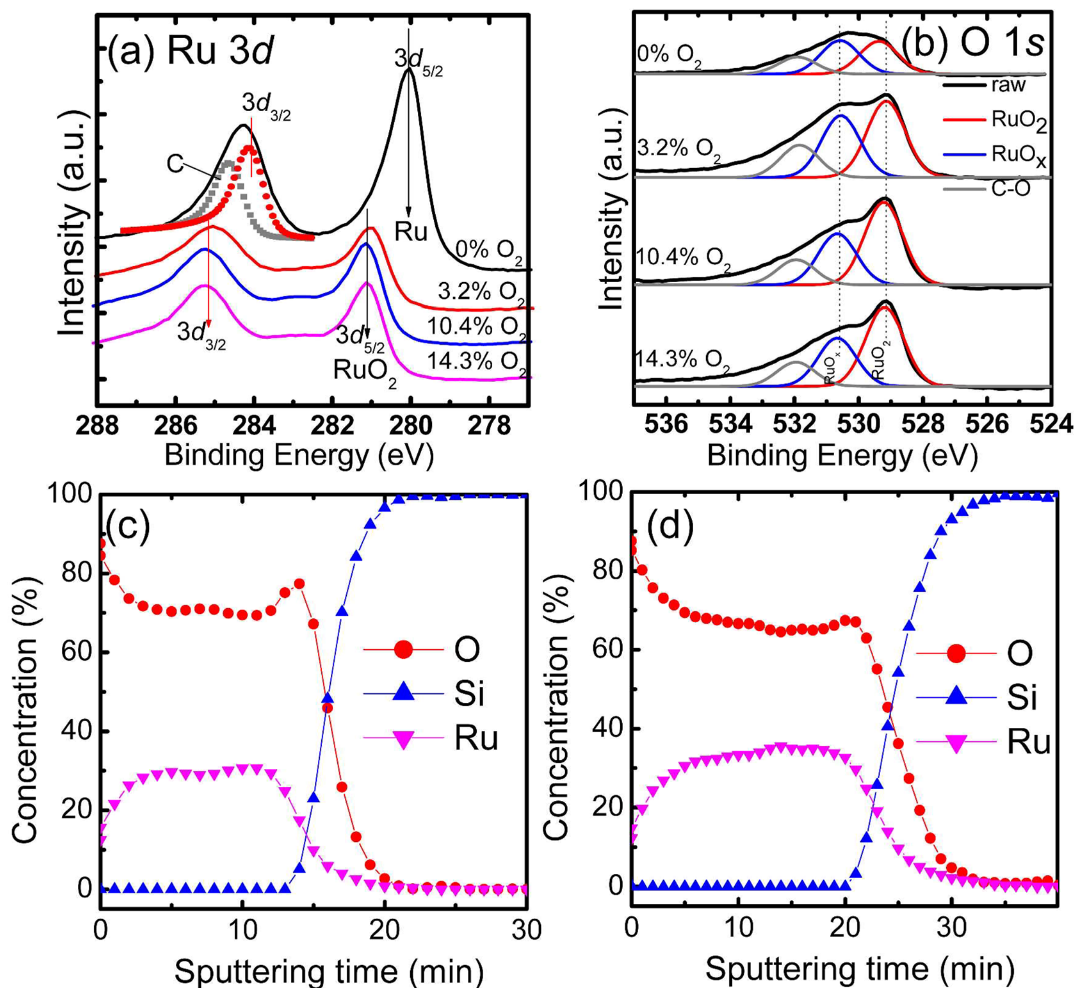

Figure 2. (a) Ru 3d and (b) O 1s regions of the XPS spectra for Ru (~10 nm) and RuO_2 (~30 nm) with various O_2 ratios on SiO_2/Si, and the AES profiles of as-deposited RuO_2 films with O_2 ratios of (c) 10.4% and (d) 14.3% on SiO_2/Si.

nm during the long induction period for RuO_2 deposition. Figure 1b shows the variations in the GAXRD spectra of the RuO_2 films according to the O_2 ratio. The deposited film was hexagonal Ru when the O_2 ratio was 0, while other films showed clear peaks corresponding to tetragonal RuO_2 phase when the O_2 ratio was > ~5%. Furthermore, the intensities of the (110) peak ($2\theta \approx 28°$) and (101) peak ($2\theta \approx 35°$) decrease and increase, respectively, with increasing O_2 ratio. The inset of Figure 1b shows the variations in the grain size of the films estimated from the two XRD peaks using the Scherrer equation ($I = k\lambda/\beta\cos\theta$, $k = 0.9$ for arbitrary particles. λ, β, and θ are the wave length, full width at half maximum, and diffraction angle, respectively).[13] It can be understood that the grain size is relatively small and constant up to the critical O_2 ratio, but abruptly increases when the O_2 ratio increases over that value, which can be understood from the lower growth rate under this condition. These results indicate that the O_2 ratio during the deposition of RuO_2 determines the growth rate as well as the growth direction and grain size of the film, which could affect the electrical properties.

The chemical properties of films deposited under O_2 ratios of 0, 3.2, 10.4, and 14.3% were estimated by XPS and AES. Panels a and b in Figure 2 show the XPS spectra of Ru 3d and O 1s peaks, respectively, for the films on SiO_2 substrate. For XPS, the Ru and RuO_2 films were ~10- and ~30-nm-thick, respectively. The XPS peak positions were calibrated using the Ru $3d_{3/2}$ and deconvoluted C 1*s* peaks (284.5 eV) from the Ru and RuO_2 samples. Figure 2a shows that the films deposited in an environment containing O_2 showed an Ru $3d_{5/2}$ peak located at ~281.2 eV, which corresponds to the binding energy of Ru $3d_{5/2}$ in RuO_2, while the film with zero O_2 ratio showed an Ru $3d_{5/2}$ peak located at ~280 eV, which corresponds to metallic Ru.[14] A slight shoulder intensity at ~281 eV suggests that the surface of the film was oxidized. The O 1*s* peaks in Fig. 2 (b) revealed slightly different oxidation states of the films, showing Ru−O bonding peaks as RuO_2 and RuO_x (possibly RuO_3) phases at the binding energies of 529.2 eV and 530.6 eV, respectively. The binding energy of O 1*s* peak in RuO_3 was reported to be 530.7 eV.[15]

Music et al. reported the presence of hyperstoichiometric RuO_3 and RuO_4 (mostly RuO_3) species during the plasma discharging using Ar and O_2 gas in the sputtering of Ru target via the mass spectrometric analysis.[16] They further revealed that the adsorption of RuO_3 onto the growing RuO_2 film is energetically stable, which further enhances the growth of RuO_2 nano-rods on the adsorbed RuO_3 islands. It was also reported that the reactively sputtered RuO_2 films have non-negligible concentration of RuO_3 as revealed by XPS.[17,18] Therefore, the observation of XPS peak at the binding energy of 530.6 eV could be ascribed to the incorporation of RuO_3.

Interestingly, the film grown at lower O_2 ratio shows a higher peak intensity at 530.6 eV, suggesting that the oxide film grown

at lower O_2 ratio contains a higher portion of less stable hyperstoichiometric oxide, which is most evidently seen in the case of 0%. This is in accordance with the estimated Ru:O ratio from the XPS peak area ratio; the atomic Ru:O ratios of the RuO_2 films with 3.2, 10.4, and 14.3% O_2 ratios were 1:1.87, 2.15, and 2.0, respectively. The hypostoichiometric composition of the RuO_2 film grown with an O_2 ratio of 3.2% could be understood from the insufficient oxygen content in the sputtering chamber. However, the higher oxygen content of the film grown at 10.4% than that of the film at 14.3% suggests that the film grown with slightly lower O_2 ratio than the critical value could have unstable structural and electrical properties as a gate metal. It appears that the RuO_2 films predominantly formed by the oxidation of Ru metal layer have a tendency to contain a hyperstoichiometric oxide component. Gou et al. reported that the metal Ru film sputtered on ALD Al_2O_3 film showed a significant concentration of RuO_3 after the annealing at 800 °C under the N_2 atmosphere.[19] This corroborates the experimental results of the present study. On the other hand, the sputtering from the oxidized target surface, which must also contain a quite high RuO_3 component, results in stoichiometric RuO_2, because the RuO_3 molecules possibly sputtered out along with the desired RuO_2 molecules from the target (of course, molecules with several other metastable oxide forms must be present too) are evacuated out due to their much higher vapor pressure. Therefore, stable stoichiometric RuO_2 film can be achieved with an O_2 ratio slightly higher than the critical value. The AES depth profiles shown in panels c and d in Figure 2 for the samples with the O_2 ratios of 10.4% and 14.3%, respectively, corroborate the XPS results. It can be understood that the RuO_2 layer with 10.4% O_2 ratio has rather higher oxygen concentration compared to that grown with 14.3%. Abe et al. claimed that at higher sputter-growth rate of RuO_2 film, the Ru atoms sputtered from the target react with oxygen on the substrate surface to form the RuO_2 films, whereas at low growth rate, RuO_2 films are deposited by the sputtering of oxidized target surface.[20] This is in accordance with the present results.

Figure 3 shows cross-section TEM images of ~30−40-nm-thick RuO_2 films with 10.4% and 14.3% O_2 ratios on a SiO_2 (6 nm)/Si stack. To reveal the different morphologies and grain shapes, wee selected somewhat thicker films for this analysis, although the actual application requires a much lower thickness. TEM of RuO_2 films on HfO_2 dielectrics could barely discern the two layers. In the case of RuO_2 grown with 10.4% O_2 ratio, the film appears to be composed of less clearly resolved columnar grains due to the possible involvement of amorphous-like regions. In contrast, the RuO_2 film grown with 14.3% O_2 ratio shows distinctive crystallization with well-developed columnar grain morphologies. Plan-view scanning electron microscopy (SEM) images shown in c and d in Figure 3 corroborate the TEM results. The larger grain size shown in images b and d in Figure 3 also coincides with the XRD data shown in the inset of Figure 1b.

Figure 4a shows the variations of V_{FB} as a function of capacitance equivalent thickness (CET) of SiO_2 dielectric for the cases of RuO_2 gate grown with O_2 ratios of 10.4% and 14.3% O_2, respectively. For comparison, the data for the Pt gate were also included. From the *y*-axis intercepts and slopes of the best-linear-fitted graphs, the work function difference (Φ_{MS}) between the gate (EWF) and Si substrate (5.1 eV), and fixed interface charge number density (Q_f), respectively, were extracted.[21] The EWF of RuO_2 on SiO_2 with 10.4% and

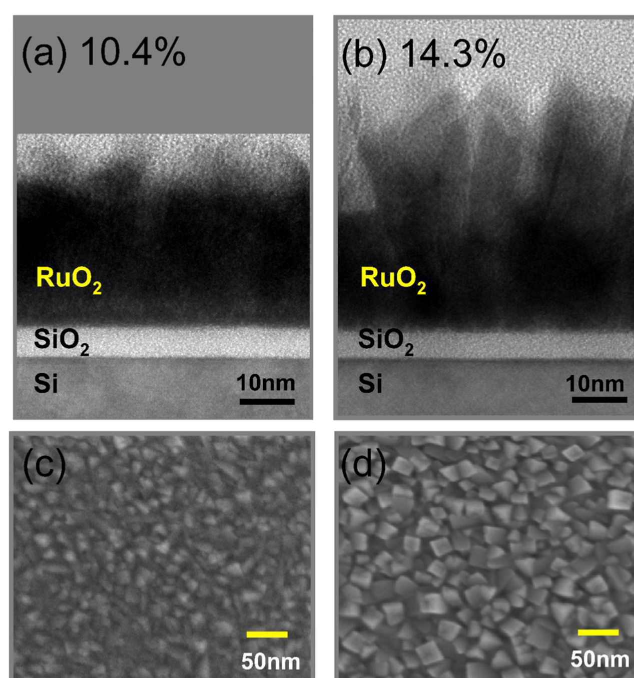

Figure 3. (a, b) Cross-section TEM, and (c, d) plan-view SEM images of RuO_2 films with O_2 ratios of (a, c) 10.4% and (b, d) 14.3% on SiO_2/Si.

14.3% O_2 ratios were estimated to be 5.29 and 5.37 eV, respectively, and that of Pt was 5.49 eV. More importantly, the Q_f levels of SiO_2 dielectrics with RuO_2 gate with 10.4% and 14.3% O_2 ratios were $\sim 3.8 \times 10^{11}$ and $\sim 1.4 \times 10^{11}$ cm^{-2}, respectively, whereas that of the Pt gate sample was as high as $\sim 1.2 \times 10^{12}$ cm^{-2}. This means that the RuO_2 film grown with the O_2 ratio of 14.3% shows an optimum performance, with sufficient EWF as the gate for p-type MOSFETs and minimized defect generation in the gate dielectric. Figure 4a also shows the variations for the samples with HfO_2 dielectrics. Due to the well-known Fermi level pinning effect, the EWFs of Pt and both RuO_2 films decreased, but lower Q_f and higher EWF were still achieved from the RuO_2 with O_2 ratio of 14.3% ($\sim 9.8 \times 10^{10}$ and $\sim 7.3 \times 10^{10}$ cm^{-2}, 5.06 and 5.19 eV for the O_2 ratios of 10.4 and 14.3%). The generally lower Q_f level for the HfO_2 compared with that of SiO_2 is due to the terraced structure of samples. HfO_2 films were deposited on the terraced SiO_2 layer, so that the damaging effect imposed to the Si/dielectric interface by the energetic bombardment during gate formation could be decreased by the HfO_2 layer.

Figure 4b shows the variation of the EOT as a function of physical oxide thickness (POT) of the HfO_2 film for the three metal gates. The bulk *k* values, estimated from the slope of the best-linear-fitted graphs, are commonly 17, and the EOTs of RuO_2-gated films are generally lower than that of Pt-gated samples by ~0.5 nm, which is in accordance with the authors' recent report.[9] The different O_2 ratio, however, did not bring about any notable difference in this EOT-POT plot. Figure 4c shows the current density (J, measured at $V_{FB} - 1$ V) vs. EOT performance. The RuO_2-gated HfO_2 films generally show a lower *J* level by approximately two orders of magnitude compared with Pt-gated films, which is probably attributed to the scaled EOT, as well as the lower damaging effect, as revealed by the lower Q_f level. However, the two different RuO_2 films did not show any notable difference in this regard, despite

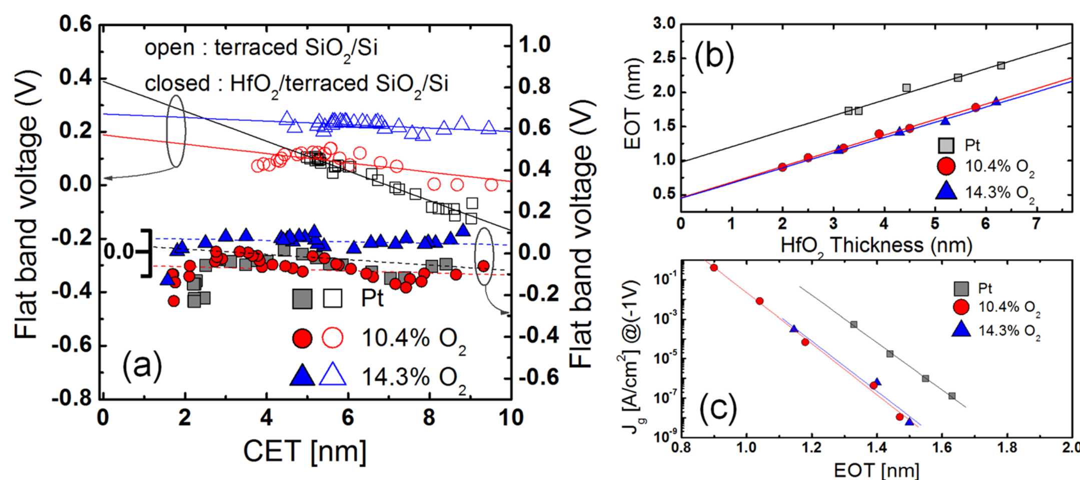

Figure 4. (a) Plot of V_{FB} vs. CET for various electrodes using terraced SiO_2 and HfO_2/thinner terraced SiO_2, (b) variation of EOT as a function of HfO_2 oxide thickness, and (c) plot of J_g vs. EOT with various electrodes on HfO_2/Si.

the different EWFs, probably due to the V_{FB} roll-off and Fermi level pinning effects.

In passing, the following must be commented on the possible origin of the EOT scaling when RuO_2 was used as the gate compared with the Pt case. This is in fact in a stark contrast to what was expected from the theoretical calculations where the Pt/high-k interface is certainly better than the conducting oxide/high-k interface in suppressing the dead-layer effect due to the better screening of polarization by the higher carrier concentration in Pt.[22] It has to be noted that the theoretical calculations already took into account the possible contribution of ionic polarization in the oxide electrode. However, almost all the experimental data have shown that the oxide electrode is better in reducing the dead-layer effect when the materials are employed in MIM (ex. ref 5), and MIS[9] configurations. This was the case even for the epitaxial Pt/$SrTiO_3$ case.[23] Therefore, it has to be concluded that there are certain factors that have not been considered in the theoretical modeling. Perhaps the most probable factor is the actual bond length between the dielectric material and electrode in the experiment. In theory, the theoretically determined equilibrium bond length was assumed. Since the distance scale under discussion (screening length) is less than 0.1 nm, only a slight deviation from the equilibrium values could make a significant deviation of the experimental results from the theoretical estimation. When the oxide electrodes are sputtered (or chemically vapor deposited) the (partly) ionic bonding natures of the dielectrics and electrode may enhance the chance for the interface to have a structure close to the theoretical intimacy. However, metals with inert nature, such as Pt, are deposited onto the dielectric surface, they may have no strong driving force to form the stable interface given the fact that the kinetic energy of the sputtered metal atoms are usually quite high. The weak chemical interaction between the oxide and Pt may also contribute to the deviation of the interface structure from the theoretical stability. Therefore, it would be an intriguing experimental (as well as theoretical) research topic to achieve a further suppressed dead-layer effect from the metal/high-k interface compared with the conducting oxide/high-k interface without invoking any experimental artifacts, such as interfacial damage or chemical reaction layer.

4. CONCLUSION

The effects of O_2 ratio during sputter-deposition of RuO_2 gate metal on the physical and electrical properties of the film and underlying gate dielectrics were examined. The growth behavior follows the well-known reactive sputtering tendency; for a given sputtering power of 60 W, ∼13% O_2 ratio was the critical level below or over which the Ru target surface is not oxidized or oxidized. According to this change in the status of the target, the RuO_2 metal gates with 10.4% and 14.3% O_2 ratio have hyperstoichiometric and stoichiometric compositions, respectively, which resulted in an EWF difference of ∼0.2 eV. The stoichiometric RuO_2 film imposed almost no damaging effects on the SiO_2 and HfO_2 gate dielectrics. The adoption of the RuO_2 gate decreased the EOT by ∼0.5 nm and the leakage current by about two orders of magnitude for the given EOT compared with the Pt-gated samples.

■ AUTHOR INFORMATION

Corresponding Author

*E-mail: cheolsh@snu.ac.kr. Tel: 82-2-882-7535.

Notes

The authors declare no competing financial interest.

■ ACKNOWLEDGMENTS

This work was supported by the Converging Research Center Program (2012K001299), and the Global Research Laboratory program (2012040157) through the National Research Foundation (NRF) of Korea.

■ REFERENCES

(1) Mistry, K.; Allen, C.; Auth, C.; Beattie, B.; Bergstrom, D.; Bost, M.; Brazier, M.; Buehler, M.; Cappellani, A.; Chau, R.; Choi, C.-H.; Ding, G.; Fischer, K.; Ghani, T.; Grover, R.; Han, W.; Hanken, D.; Hattendorf, M.; He, J.; Hicks, J.; Huessner, R.; Ingerly, D.; Jain, P.; James, R.; Jong, L.; Joshi, S.Kenyon, C.; Kuhn, K.; Lee, K.; Liu, H.; Maiz, J.; Mclntyre, B.; Moon, P.; Neirynck, J.; Pae, S.; Parker, C.; Parsons, D.; Prasad, C.; Pipes, L.; Prince, M.; Ranade, P.; Reynolds, T.; Sandford, J.; Shifren, L.; Sebastian, J.; Seiple, J.; Simon, D.; Sivakumar, S.; Smith, P.; Thomas, C.; Troeger, T.; Vandervoorn, P.; Williams, S.; Zawadzki, K. *Technical Digest of 2007 International Electron Devices Meeting Technical Digest*; IEEE: Piscataway, NJ, 2007; pp 247−250.
(2) Choi, C.; Lee, J. C. *J. Appl. Phys.* **2010**, *108*, 064107.
(3) Kim, H. K.; Lee, S. Y.; Yu, I.-H.; Park, T. J.; Choi, R.; Hwang, C. S. *IEEE Electron Dev. Lett.* **2012**, *33*, 955−957.

(4) Li, Q.; Patel, C.; Ardebili, H. *Int. J. Smart Nano Mater.* **2012**, *3*, 23−32.
(5) Hwang, C. S. *J. Appl. Phys.* **2002**, *92*, 432−437.
(6) Pertsev, N. A.; Dittmann, R.; Plonka, R.; Waser, R. *J. Appl. Phys.* **2007**, *101*, 074102.
(7) Gerra, G.; Tagantsev, A. K.; Setter, N.; Parlinski, K. *Phys. Rev. Lett.* **2006**, *96*, 107603.
(8) Han, J. H.; Han, S.; Lee, W.; Lee, S. W.; Kim, S. K.; Gatineau, J.; Dussarrat, C.; Hwang, C. S. *Appl. Phys. Lett.* **2011**, *99*, 022901.
(9) Kim, H. K.; Yu, I.-H.; Lee, J. H.; Park, T. J.; Hwang, C. S. *Appl. Phys. Lett.* **2012**, *101*, 172901.
(10) Malkomes, N.; Vergohl, M. *J. Appl. Phys.* **2001**, *89*, 732−739.
(11) Hauser, J. R.; Ahmed, K. *AIP Conf. Proc.* **1998**, *449*, 235−239.
(12) Kusano, E.; Kinbara, A. *J. Appl. Phys.* **2000**, *87*, 2015−2019.
(13) Khan, Z. H.; Islamuddin; Kumar, R. K.; Salah, N.; Habib, S.; Abdallah El-Hamidy, S. M.; Rafat, M.; Husain, M. *Int. J. Nanosci.* **2010**, *9*, 423−429.
(14) Madhavaram, H.; Idriss, H.; Wendt, S.; Kim, Y. D.; Knapp, M.; Over, H.; Assmann, J.; Loffler, E.; Muhler, M. J. *J. Catal.* **2001**, *202*, 296−307.
(15) *NIST, X-ray Photoelectron Spectroscopy Database*; http://srdata.nist.gov/xps/ (accessed on Jan. 25, 2013).
(16) Music, D.; Breunung, J.; Mráz, S.; Schneider, J. M. *Appl. Phys. Lett.* **2012**, *100*, 033108.
(17) Lin, Y.-T.; Chen, C.-Y.; Hsiung, Chang-Po; Cheng, K.-W.; Gan, J.-Y. *Appl. Phys. Lett.* **2006**, *89*, 063123.
(18) Music, D.; Basse, F. H.-U.; Haßdorf, R.; Schneider, J. M. *J. Appl. Phys.* **2010**, *108*, 013707.
(19) Gou, H.-Y.; Ding, S.-J.; Huang, Y.; Sun, Q. Q.; Zhang, W.; Wang, P.-F.; Chen, Z. *J. Electron. Mater.* **2010**, *39*, 1343.
(20) Abe, Y.; Kaga, Y.; Kawamura, M.; Sasaki, K. *J. Vac. Sci. Technol. B* **2000**, *18*, 1348−1351.
(21) Wen, H.-C.; Choi, R.; Brown, G. A.; Bosche, T.; Mattews, K.; Harris, H. R.; Choi, K.; Alshareef, H. N.; Luan, H.; Bersuker, G.; Majhi, P.; Kwong, D.-L.; Lee, B. H. *IEEE Electron Dev. Lett.* **2006**, *27*, 598−601.
(22) Stengel, M.; Spaldin, N. *Nature* **2006**, *443*, 679−682.
(23) Boesch, D. S.; Son, J.; LeBeau, J. M.; Cagnon, J.; Stemmer, S. *Appl. Phys. Exp.* **2008**, *1*, 091602.